Nat Hazards (2008) 47:1–16
DOI 10.1007/s11069-007-9211-5

ORIGINAL PAPER

Results of geodetic and geotechnical monitoring of subsidence for Taiwan High Speed Rail operation

Cheinway Hwang · Wei-Chia Hung · Chih-Hsi Liu

Received: 13 May 2007 / Accepted: 5 October 2007 / Published online: 12 March 2008

Abstract Taiwan High Speed Rail (THSR), which began operations in January 2007, passes through an area in Yunlin County where the largest cumulative subsidence measured during 1992–2006 exceeds 100 cm. Leveling benchmarks, GPS pillars and multi-level monitoring wells were deployed in this area to collect detailed subsidence data from October 2003 to 2006. Leveling is carried out on both ground benchmarks and survey bolts attached to THSR columns. Minimum constraint solutions of leveling networks produce estimated heights accurate to a few mm. Special attention is paid to code smoothing, ionospheric, tropospheric and ocean tidal loading (OTL) effects, so that height estimates from GPS are optimal. Leveling and GPS-derived height changes are consistent to 1 cm, and show that from Stations 210 to 240K of TSHR, the subsidence is bowl shaped. Measurements of sediment compaction in specific depth intervals at three monitoring wells indicate that most of the subsidence is caused by sediment compaction at depths from 50 to 300 m. The major compaction occurs in the interval 220–300 m and is attributed to ground water withdrawal. Large angular deflections as determined from subsidence measurements are detected at some columns, but are below the upper bound (1/1,000) of tolerance specified in the safety code. With the current subsidence and sediment compaction, no significantly reduced loading capacity of the columns is expected to occur. For a safe THSR operation, subsidence and sediment-compaction monitoring should be continued, and current ground water withdrawal in Yunlin must be reduced or stopped.

Keywords GPS · Leveling · Monitoring well · Subsidence · THSR

C. Hwang (✉) · W.-C. Hung
Department of Civil Engineering, National Chiao Tung University,
1001 Ta Hsueh Road, Hsinchu 300, Taiwan
e-mail: cheinway@mail.nctu.edu.tw

W.-C. Hung · C.-H. Liu
Energy and Resources Laboratory, Industrial Technology Research Institute,
Building 24,195, Sec. 4, Chunghsing Road, Chutung, Hsinchu, Taiwan

1 Introduction

Taiwan High Speed Rail (THSR) is one of the most important national infrastructures in Taiwan. THSR began operations in January 2007 and is the first build-operation-transfer (BOT) case in the Department of Transportation, Taiwan. THSR has a total length of 345 km with 11 stations (seven operational, four planned; see Fig. 1), and costs an

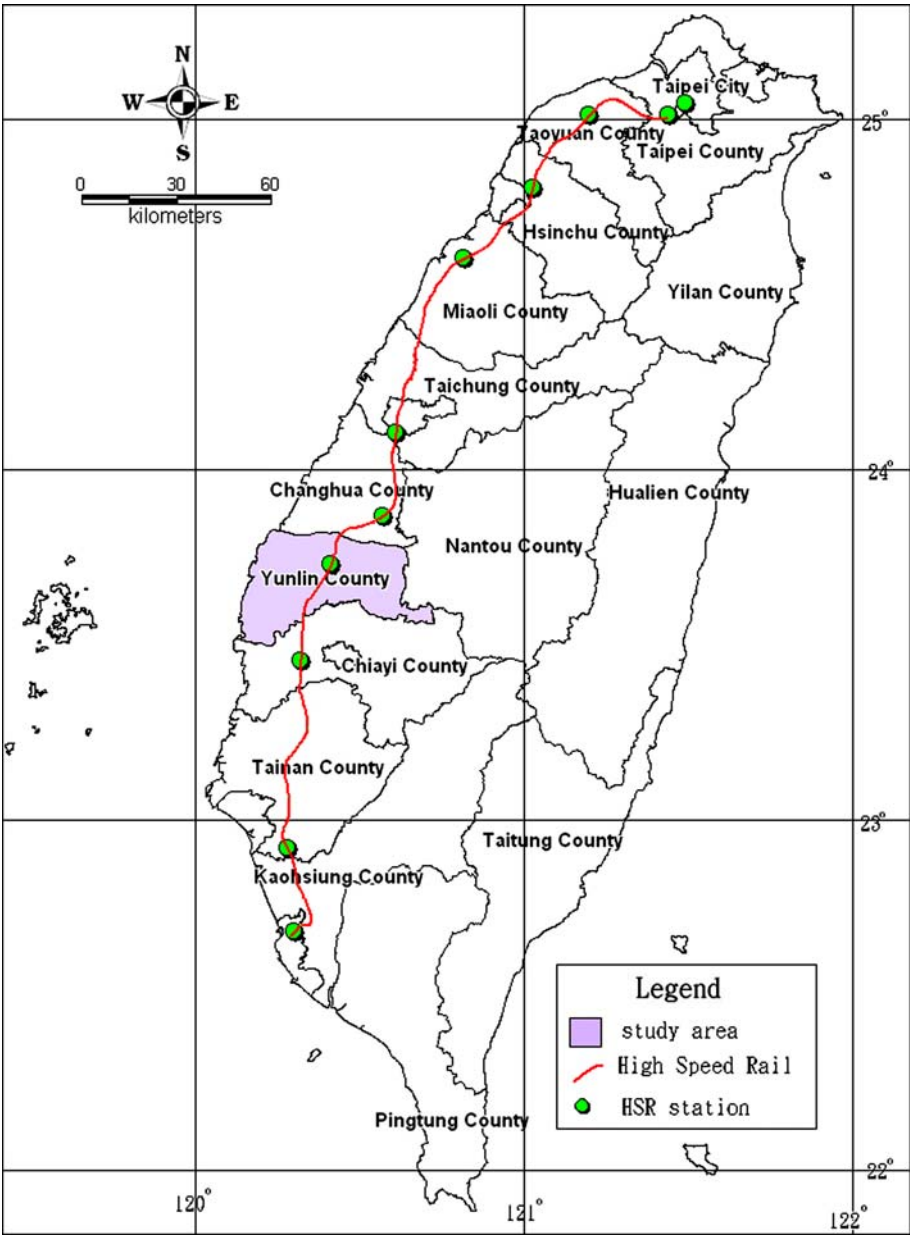

Fig. 1 Route of THSR, its maintenance facility and rail stations

estimated USD 15 billion. THSR operates at an average speed of 300 km/h and achieves a top speed of 350 km/h. Due to the high speed, the safety codes for THSR are stringent. For example, one safety code demands that the angular deflection (see Sect. 4) at any supporting column of the THSR rail cannot exceed 1/1,000.

THSR passes through an alluvial fan south of Choshui River, where ground water used to be abundant before excessive pumping for agricultural use. This area is largely in Yunlin County. The pumping of ground water has resulted in land subsidence. According to Liu and Hung (2006), from 1992 to 2006 the largest cumulative subsidence in Yunlin is more than 100 cm (Fig. 2). From 2005 to 2006, the maximum subsidence is more than 10 cm (Fig. 3). Despite governmental measures, the problem of subsidence continues today. The impact of subsidence on THSR safety depends on the depth of sediment compaction. Subsidence is a result of sediment compaction. For any column, sediment compaction above the foundation of the column will introduce a negative friction force that reduces the loading capacity of the column. If the sediment compaction occurs below the foundation, the column and the rail will subside to create angular deflection. Since the foundation of a column is 70 m deep, measurements of sediment compaction at different depths are needed to determine friction forces and angular deflections.

Motivated by the need for subsidence information for THSR, in this article we focus on monitoring subsidence around a section of THSR in Yunlin (Figs. 2 and 3). Ideal monitoring sensors will be able to collect data at surface and sub-surface locations. We choose to use GPS and leveling to determine surface subsidence, as was done in many similar works (e.g., Abidin et al. 2001; Liu et al. 2004; Teatini et al. 2005; Motagh et al. 2007). In order to determine sub-surface sediment compaction at different depths, we choose to use multi-level monitoring wells. A monitoring well can be used to determine sediment properties and compaction at different depths and identify the mechanism of subsidence. An early, similar

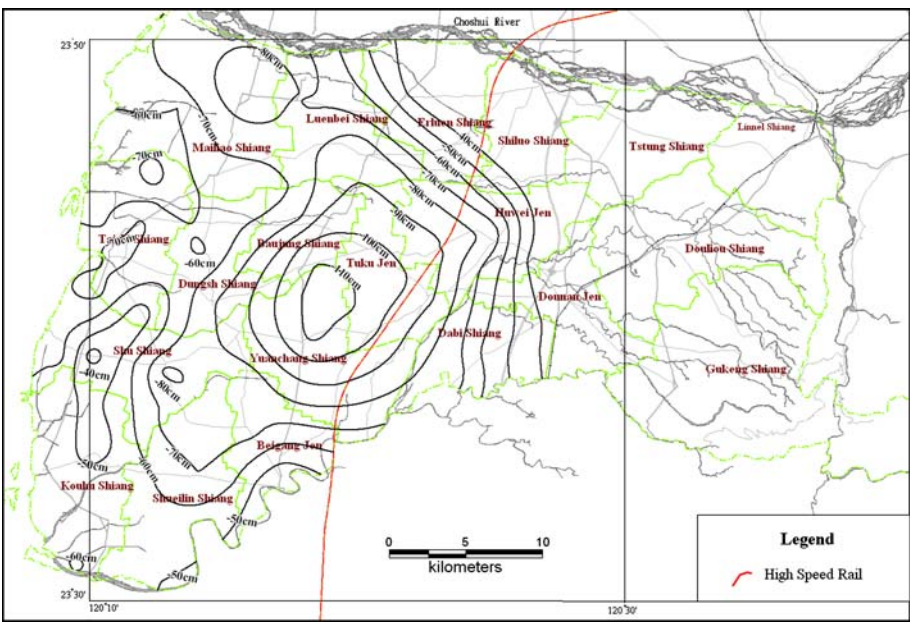

Fig. 2 Cumulative subsidence in Yunlin from 1992 to 2006

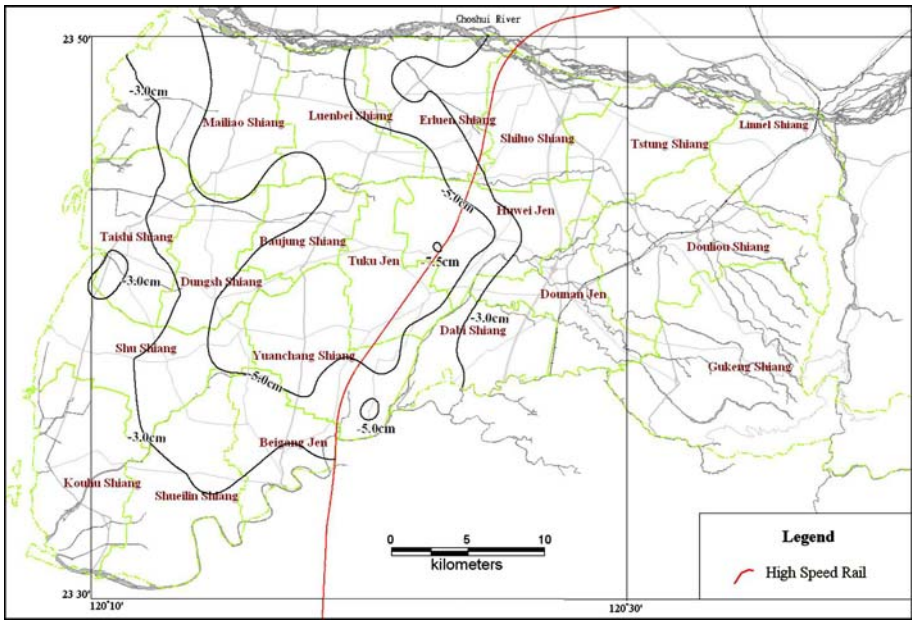

Fig. 3 Subsidence in Yunlin from 2005 to 2006

work was carried out by Liu et al. (2004), who studied subsidence and its mechanism in an area north of Yunlin. This article will focus on monitoring subsidence in a section of THSR in Yunlin and investigate the impact of subsidence on the safety of THSR operation.

2 Monitoring sensors and data processing

2.1 Leveling

Figure 4 shows the distributions of leveling networks, GPS pillars and monitoring wells used in this article. Figure 5 shows sample pictures of these sensors. In addition to the THSR leveling network, a leveling network west of THSR was established by Water Resource Agency (WRA) of Taiwan to monitor surface subsidence in Yunlin County. Based on early repeat leveling results, the elevation of WR12 is stable and its elevation is used in the minimum constraint solution of the leveling network adjustment below. WR12 is a benchmark located east of the No. 1 Freeway (Fig. 4). With 10 major leveling lines, the length of the THSR leveling network is 120 km and consists of two major loops: a loop formed by Lines 2, 10, 3, 4, and 5 in the north, and a loop formed by Lines 4, 7, and 6 in the south. Along Lines 3, 7, and 10 around the THSR rail, the benchmarks on the ground are spaced at a 1-km interval. Along these leveling lines, a survey bolt is mounted on each column of the rail to determine column subsidence and in turn angular deflection (Fig. 5). The elevations of all ground benchmarks and column survey bolts were measured in four campaigns from October 2003 to 2006.

The accuracy requirement for the leveling is a $3\sqrt{K}$ mm misclosure in any double run, where K is the distance between two neighboring benchmarks in km. At each leveling

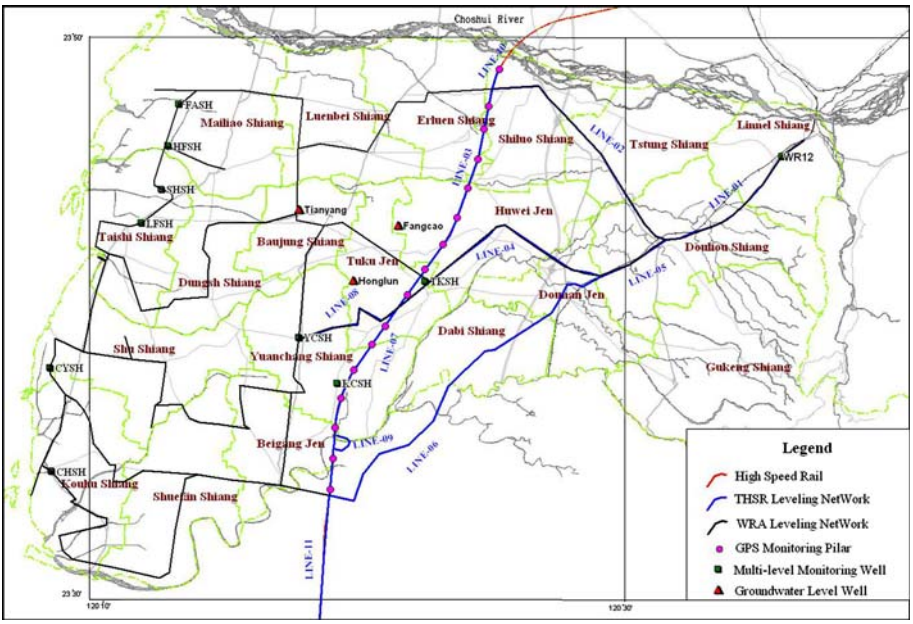

Fig. 4 Distributions of leveling networks, GPS pillars and monitoring wells in Yunlin

setup, the distances to the foresight and backsight were measured by an electronic distance measurement (EDM) device to ensure the two are identical. Corrections for collimation error, atmospheric refraction and the earth's curvature were applied to the differential heights (Wolf and Ghilani 2005). Since the cumulative differences between foresight and backsight distances do not exceed 10 m, residual collimation errors, the earth's curvature and atmospheric effects were negligible. Since we used INVAR leveling rods, temperature correction was negligible. Since the study area is flat, no orthometric correction was needed (Hwang and Hsiao 2003).

The corrected height differences from leveling were least squares adjusted to determine the heights. In the adjustment, the observation equation of a height difference is

$$\Delta h_{ij} + V_{ij} = H_j - H_i, \quad \text{weight} = P_{ij} \tag{1}$$

where Δh_{ij} is height difference, V_{ij} is residual, H_i and H_j are elevations at benchmarks i and j, and P_{ij} is weight. We use the inverse distance between two benchmarks as the weight. A matrix representation for all height differences is

$$\mathbf{L} + \mathbf{V} = \mathbf{AX}, \quad \text{weight matrix} = \mathbf{P} \tag{2}$$

where vectors **L**, **V**, and **X** contain height differences, residuals and heights and **A** is the design matrix. The least-squares solution of (2) is

$$\mathbf{X} = (\mathbf{A^T PA})^{-1}(\mathbf{A^T PL}) \tag{3}$$

In (3), we have employed a minimum constraint solution by holding fixed the height of WR12. In order to ensure the quality of least-squares solution, we screen the observables for outliers using Baada's data snooping technique (Koch 1987; Caspary 1987). First the standardized residual of an observable is computed as

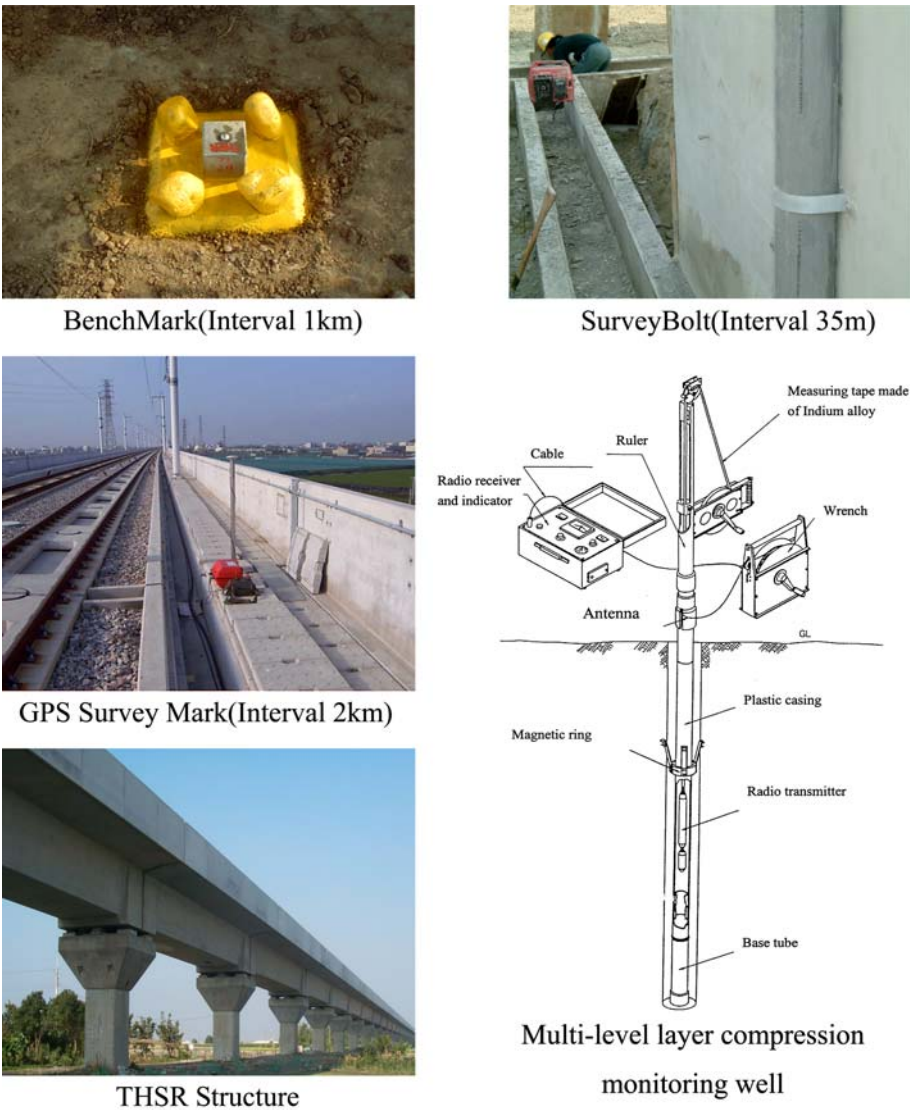

Fig. 5 Sample pictures of monitoring sensors. The point intervals for leveling benchmarks, survey bolts, and GPS pillars are 1 km, 35 m, and 2 km, respectively

$$Wi = \frac{V_i}{\delta V_i} \tag{4}$$

where δV_i is the standard error of residual V_i, which is the squared root of a diagonal element of matrix $\mathbf{Q_v}$ as follows

$$\mathbf{Q_v} = \mathbf{P^{-1}} - \mathbf{A}(\mathbf{A^T P A})^{-1}\mathbf{A^T} \tag{5}$$

With a significance level of 0.01, the critical value for data snooping in (4) is 3.3. That is, if $W_i > 3.3$, the observable (height difference) associated with V_i is regarded as an outlier and is removed from the input to the adjustment. A second adjustment is then performed

without these outliers. Since all misclosures are smaller than $3\sqrt{K}$ mm and all raw data are carefully inspected, we did not find any outliers in the data from the three campaigns. The average standard errors of point elevations for all campaigns are below 3 mm, and the largest standard error is 7 mm.

2.2 GPS

GPS is also used as an independent tool for monitoring subsidence. Unlike leveling, it is flexible to choose measurement sites and each GPS site works independently from the others in data collection. We established 16 GPS survey pillars at the sidewalk of the THSR rail at a 2-km interval along a section of the rail overlapping with the leveling profile (Fig. 4). Performing leveling on the rail will be difficult and inaccurate because the rail is elevated (Fig. 5). A total of 16 GPS pillars were mounted and are named YL01, YL02, … ,YL16. Six GPS measuring campaigns (October 2003, April 2004, October 2004, April 2005, October 2005, and October 2006) were carried out using a Leica System 500 GPS receiver with an AT503 antenna. Each pillar was occupied from 10 PM to 8 AM the next day for two consecutive days, yielding a total of 20 h of data. The pillar is so designed that the GPS antenna attached to a pole can be force centered to the same location (Fig. 5). Such a design fulfills the requirement set by the National Geodetic Survey (NGS) 58 standard (Zilkoski et al. 1997), which states that, in order to achieve a 2-cm accuracy in positioning, repeat GPS measurements must use forced centering.

The GPS data processing software Bernese 4.2 (Beutler et al. 2001) was used to determine the pillar coordinates using the ionosphere-free L3 phase combination. The final IGS GPS satellite ephemerides (http://www.igscb.jpl.nasa.gov/components/prods_cb.html) were used in the coordinate determination. Careful modeling of tropospheric delay is essential for accurate determination of height in GPS positioning (Dodson et al. 1996). For the tropospheric delay, we used the Saastamoinen model and took into account the zenith-dependent variation of tropospheric delay (Leick 2004). Specifically, for each station we estimated a zenith delay parameter every 2 h.

In the GPS data processing, the C/A codes were smoothed before estimating integer ambiguities. Smoothing was done on subsets or sub-sessions of GPS data and the smoothed codes were combined to form the final, smoothed codes for the entire session. Using the narrow-lane phase combination (Leick 2004), spurious phase observables that exceeded four times of the standard error were removed. Ocean tidal loading (OTL) corrections based on the Bos and Scherneck model (http://www.oso.chalmers.se/%7Eloading/index.html) were applied to the GPS measurements. Similar to the pattern of ocean tides in Taiwan Strait, The OTL effect on GPS height is the largest (about few cm in amplitude for the semi-diurnal component) in the central, western coasts of Taiwan (near the study area), and decreases toward the north and the south. The phase center offsets and variations of antennas adopted from NGS were applied in the GPS solutions. The multi-path effect on GPS height is negligible because the antennas were well above the ground and there was no obstruction nearby. With 20 h of GPS data and using careful data processing, the formal standard errors of estimated ellipsoidal heights of pillars in all the campaigns are at the mm level. This accuracy will be validated by the leveling result in Sect. 3.1.

In this article, GPS data were collected in a “campaign” mode. For areas with large subsidence and of special interest, a “continuous” mode of GPS data collection should be considered. Continuous GPS data can be used to compute elevation changes on a daily basis. Some continuous GPS sites can even collect high-rate data (e.g., 1 Hz sampling rate)

to determine real-time deformation of columns during episodic events such as earthquakes or typhoons.

2.3 Multi-level monitoring well

Most land subsidence in Yunlin County is caused by withdrawal of ground water. The reduction of pore-fluid pressure accompanying ground water extraction results in increased intergranular stress (effective stress) of the sediments and in turn compresses the sediment. Sediment compaction leads to surface subsidence. The extent of compaction is normally correlated with depth. In order to measure compaction at different depths, three 300-m deep boreholes, named TKSH, YCSH, and KCSH, were drilled at locations shown in Fig. 4. The TKSH borehole is closest to THSR at a distance of 0.5 km, and the result is more representative of the sediment compaction along THSR than the other two boreholes. Since the sediments are stratified, it is advantageous to measure compaction in multiple depth intervals in the boreholes. This was accomplished using multi-level magnetic rings to measure compaction along the boreholes (Laier and Brenner 1984; Liu et al. 2004). First, the sediment types at different depths were determined by natural gamma and resistivity at the three boreholes (Table 1). The number of deployed magnetic rings depends on the sediment strata in the borehole and the expected resolution of the estimated compaction. Based on the sediment types, 21–26 magnetic rings were deployed in each borehole (Table 1). The magnetic rings are anchored to the wall of the borehole (Fig. 5).

In order to measure the depth of a magnetic ring, a sensor attached to an indium-alloy tape was lowered into the borehole. Upon reaching the center of a magnetic ring, the electric current of the sensor, as indicted in a radio transmitter, will be zero, and the depth of this ring below a reference datum is determined. The measurement of the ring depth is accurate to 1 mm. Repeat measurements of the ring depth yield information about the compaction of the ring. On average, ring depths at the three boreholes were measured monthly.

3 Results

3.1 Subsidence from leveling and GPS

Figure 6 shows the cumulative subsidence from leveling and GPS relative to epoch October 2003 from Stations 210 to 240K. Since the benchmarks on the ground were

Table 1 Major information about monitoring wells

Well	TKSH	YCSH	KCSH
Nearest station	224K + 189	231K + 500	232K + 470
Distance to THSR (km)	0.5	2.5	0.6
No. of magnetic rings	26	26	21
Sediment types	(1) 0–150 m: sand layer (2) 150–300 m: silt and clay (3) 220–300 m: interlayers of silt and silty clay	(1) 0–50 m: silt and silty clay (2) 50–300 m: interlayers of sand, silt and clay	0–300 m: interlayers of sand and silty clay

destroyed frequently due to the construction of THSR, only few benchmarks have continuous records during the period October 2003–2006. Thus, the leveling results in Fig. 6 are associated with the heights at the survey bolts on the THSR columns. Since GPS pillars are mounted on the THSR structure, both the height changes at the bolts and pillars are indicative of subsidence attributed to sediment compaction occurring below the foundations of columns. Relatively large discrepancies (up to 3 cm) between GPS and leveling heights are found near Stations 212, 214, and 216K, and are mainly due to GPS signal obstructions here. Re-locations of these GPS pillars should be considered in future GPS campaigns. Excluding these large discrepancies, the GPS and leveling-derived subsidence are consistent to 1 cm, showing that GPS is a reliable tool for monitoring subsidence here. This agreement also serves as a cross-validation for both sensors.

Around Stations 219K and 224K + 200, subsidence is anomalously large, and is due to construction works here. The subsidence along the THSR section in Fig. 6 is roughly bowl-shaped, with the bottom of the bowl at Stations 218–236K. Based on the magnitude and the slope of subsidence, three types of subsidence are recognized:

(1) *Minor subsidence: Stations 210–216K and 236–240K* These sections have a minor subsidence rate of less than 3 cm/year. Here the slope is gentle, so small angular deflections are expected.

(2) *Moderate subsidence: Stations 216–222K* The section is 6 km long and the cumulative subsidence ranges from 5 to 22 cm. The slopes of subsidence are relatively large compared to others. Here angular deflections will be significant (see Sect. 4).

(3) *Major subsidence: Stations 218–236K* Here, the subsidence rate is the largest, and is more than 5 cm/year. The subsidence is uniform along this section. Since the slopes are smooth, small angular deflections are expected.

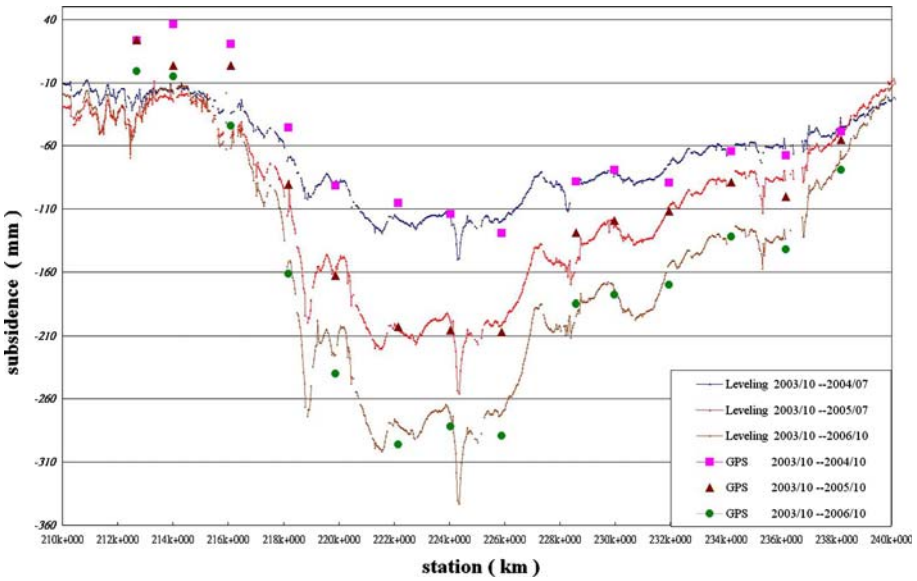

Fig. 6 Subsidence from GPS and leveling with respect to THSR stations

3.2 Compaction at different depths from monitoring wells

Table 2 summarizes the compaction measured at the three monitoring wells. The total compaction measured in each well is equivalent to land subsidence at each site assuming all the compaction occurs in the measured intervals in the wells. Only at YCSH (2.5 km to THSR) does measured compaction include the near surface. All major compaction occurs below 200 m, and the depths of minor compaction vary. In the major compaction zone, the variation of compaction relative to depth is rapid, while in the minor compaction zone the variation is slow. YCSH has the largest ratio of compaction in the shallow interval (0–70 m) to total compaction, and TKSH (0.5 km to THSR) has the least ratio. The trends of compaction from the three monitoring wells are similar to that of subsidence from leveling and GPS (Fig. 6). That is, subsidence is the largest at Station 224K + 189 (near TKSH) from both leveling and the cumulative compaction in monitoring wells, and it decreases as the station number increases (finishing at station near KCSH).

As an example, Fig. 7 shows the sediment types and compaction with respect to depth at the TKSH monitoring well. The sedimentary strata at TKSH contain inter-bedded clays, silts, fine-to-coarse sands, and gravels. Here compaction occurs only between 50 and 300 m, and is evident in the intervals 86–156 m, 172–185 m, and 220–300 m. The largest compaction occurs in the interval 220–300 m. In order to identify the mechanism of the compaction in the interval 220–300 m, in Fig. 8, we compare the cumulative compaction and changes of ground water level at the depths of 225 m (Honglun well) and 284 m (Tianyang well). The locations of Honglun and Tianyang ground water level monitoring wells are given in Fig. 4. As shown in Fig. 8, from July 1999 to July 2004 the ground water levels at Honglun and Tianyang wells decreased steadily and these declines lead to the sediment compaction at TKSH (our records of compaction began in October 2003). The correlation between compaction and water level in Fig. 8 suggests that withdrawal of ground water is responsible for the major sediment compaction at layers 220–300 m.

Figure 9 shows the stress–strain relationship near the Honglun and Tianyang wells. In Fig. 9, once a strain is built up by stress, reduction of stress will not lead to reduction of strain. Therefore, the compactions at Honglun and Tianyang are mostly inelastic and the inelastic subsidence near these wells will be permanent. Since much of the sediment compaction is attributed to hydrodynamic lag or residual compaction (Terzaghi et al. 1996), increased ground water level will not stop sediment compaction. Therefore, the compaction at TKSH continues from July 2004 to the present day (October 2007) despite increased ground water level since July 2004. In order to quantify the residual compactions, we compute the time constant needed to complete 90% compaction, t, using the formula (Terzaghi et al. 1996)

Table 2 A summary of compaction measured at three monitoring wells

Monitoring well	TKSH	YCSH	KCSH
Depth of major compaction (m)	220–300	200–300	250–300
Depth of minor compaction (m)	50–220	0–200	100–250
Ratio of compaction at 0–70 m over total (%)	3	14	6
Cumulative compaction from October 2003 to 2006 (cm)	−21.9	−20.9	−13.2

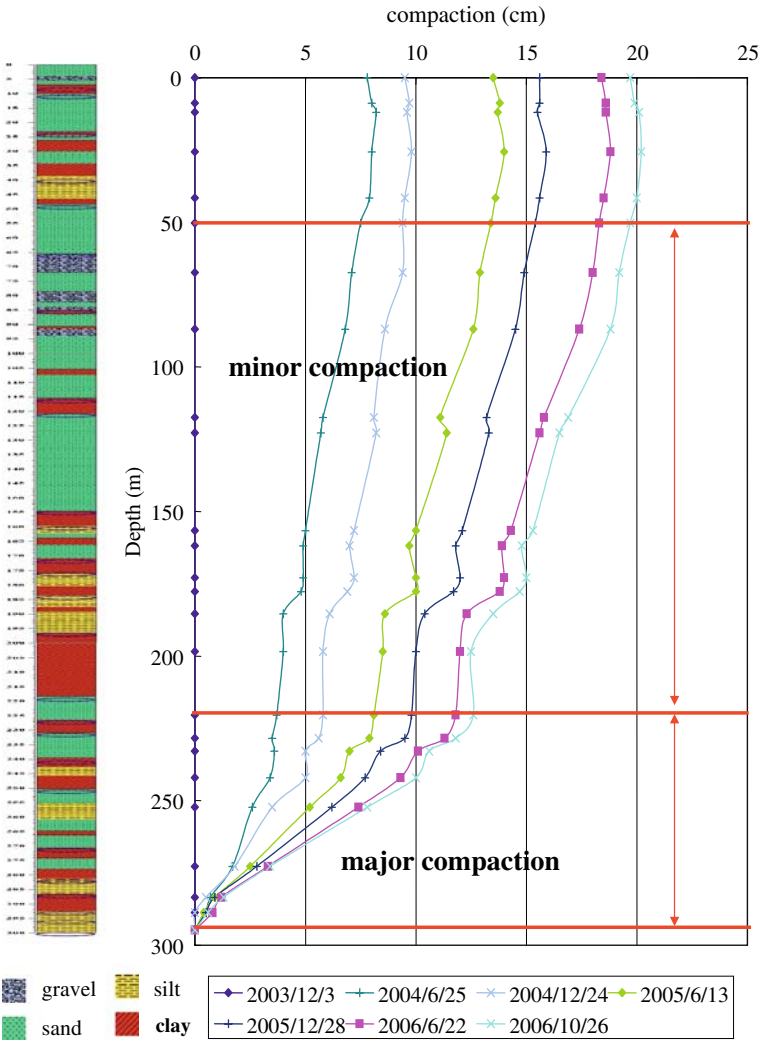

Fig. 7 Sediment type and cumulative compaction (starting from October 2003) at the TKSH monitoring well

$$t = \frac{T_v H^2}{4C_v} \tag{6}$$

where C_v is coefficient of compaction, H is thickness and T_v is a constant. Based on the experiments of Lin and Chan (1997) in Yunlin, we adopt $C_v = 0.00181$ cm^2/s and $T_v = 0.848$. The time constant t in Eq. 6 is also the time for the confining units to equilibrate to the head of the surrounding aquifer. Table 3 lists the time constants for completing 90% of compaction at seven layers of the significant compaction zone at TKSH. The time constants range from 26 to 488 days, and mostly exceed 4 months. The time constants help to explain the behavior of compaction with respect to ground water level in Fig. 8. Furthermore, from October 2003 to October 2006, the cumulative

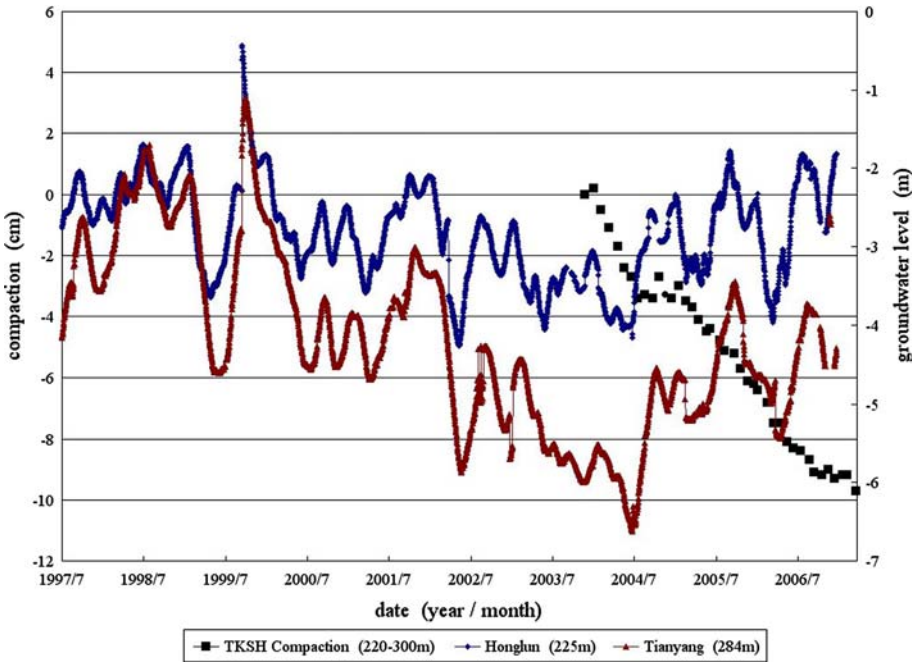

Fig. 8 Cumulative compaction measured at depths greater than 220 m and ground water level at the TKSH monitoring well

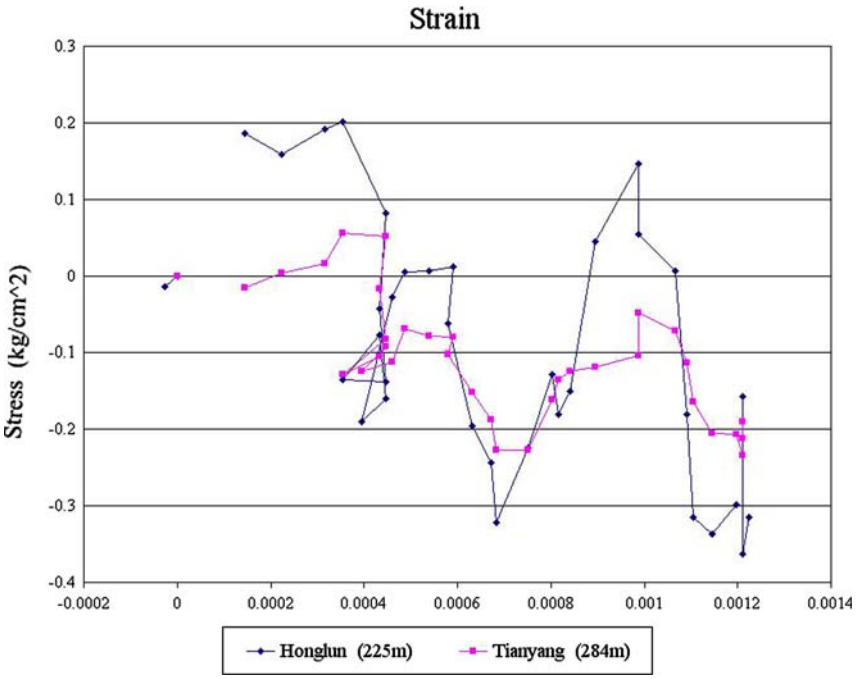

Fig. 9 Stress and strain at the TKSH monitoring well

Table 3 Time constants for 90% compaction at the significant compaction zone of the TKSH well

Layer[a]	Depth (m)	Thickness (m)	Time constant (day)
1	226.5–230.9	4.4	263
2	239.5–242.6	3.1	130
3	245.8–250.3	4.5	275
4	264.8–266.2	1.4	27
5	270.5–274.2	3.7	186
6	277.9–281.2	3.3	148
7	286.5–292.5	6	488

[a] A layer contains sediment materials of the same property

subsidence at Station 224K + 189 (near TKSH) from leveling is 33.5 cm, which is larger than the compaction of 21.9 cm measured in the TKSH monitoring well. This suggests that, at TKSH some sediment compaction below 300 m also may have occurred. This observation is supported by the fact that a water company has constructed 10 wells near TKSH to withdraw ground water below 300 m during October 2003–2006.

In order to understand the role of rainfall in sediment compaction, in Fig. 10 we show the relationship among sediment compaction, ground water level, and daily rainfall at TKSH. We notice that, just after a large rainfall the ground water levels at the Honglun and Fangcao wells increase steadily for few days and then drop. Increased ground water level has slowed down sediment compaction (this is seen as a decrease of cumulative compaction after a large rainfall in Fig. 10; for example see the curves around August 26, 2004). Such a fast response of sediment compaction to ground water level change suggests that the subsidence problem in Yunlin can be improved if withdrawal of ground water is

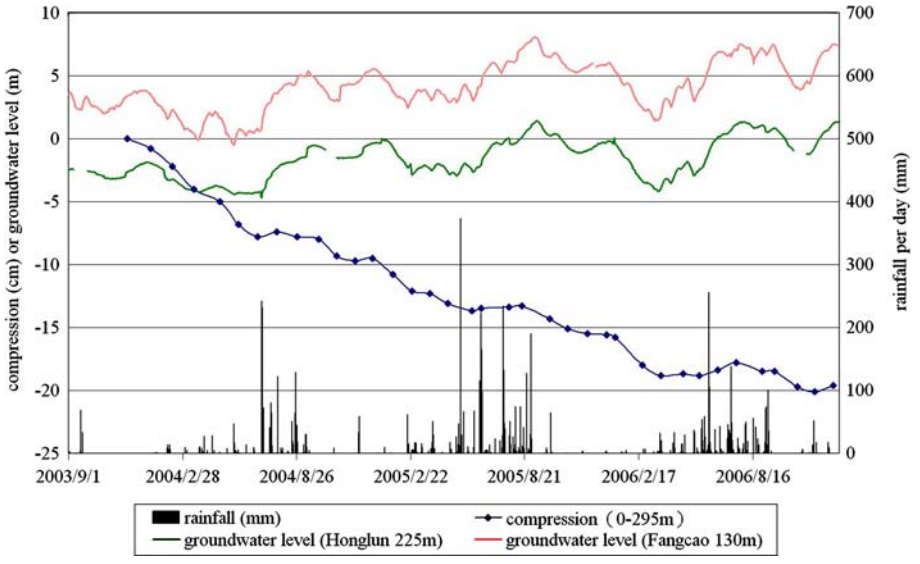

Fig. 10 Sediment compaction, daily ground water level and rainfall at the TKSH monitoring well

stopped or decreased. In addition, managed artificial recharge of ground water may help to reduce subsidence in just a short time.

4 Implication of subsidence for THSR operation

The most important outcome of subsidence measurements in this article is angular deflection. Subsidence will create angular deflection that will damage the THSR rail. The angular deflection at the nth column is defined as

$$\theta_n = \left| \frac{\delta_n - \delta_{n-1}}{L_n} + \frac{\delta_n - \delta_{n+1}}{L_{n+1}} \right| \tag{7}$$

where δ_{n-1}, δ_n, δ_{n+1} are the subsidence at three consecutive columns $n - 1$, n, $n + 1$, and L_n, L_{n+1} are the horizontal distances from the nth column to the $(n - 1)$ and $(n + 1)$th columns, respectively. For a safe operation, it is required that $\theta_n < 1/1{,}000$. Using the subsidence derived from leveling (Fig. 6), we have estimated angular deflections at all columns from Stations 210 to 240K. Due to an agreement with the funding agencies of this research (National Science Council and Water Resource Agency, Taiwan), we cannot publish the estimated angular deflections along the studied THSR section in this article. We find that all angular deflections are smaller than 1/1,000. The largest angular deflection is 0.8/1,000 and is near Station 224K + 300, where THSR intersects a west–east expressway. The large angular deflection is clearly due to construction work here, and will soon become small when the work is completed. Furthermore, a device below the THSR rail can be used to adjust the height of the rail to compensate the subsidence, provided that the subsidence does not exceed the limit of adjustment. In order to properly adjust the height of the rail, knowledge of angular deflection must be available and this is based on the measured subsidence of individual columns.

Another risk of subsidence is reduction of column loading capacity. According to the design specifications of THSR, a subsidence rate of more than 4 cm/year between land surface and the depth of the foundation of column (70 m) will create a frictional force that will reduce the loading capacity of a column. From Sect. 3.1, we find that only few columns between Stations 218 and 236K have subsidence rates larger than 4 cm/year. However, here the subsidence occurs below the foundations of the columns. Therefore, currently reduction of column loading capacity will not occur between Stations 210 and 240K.

Safety is a major concern of THSR customers. The public in Taiwan have long been aware of the fact that land subsidence exists in most cities of western Taiwan. The subsidence problem in Yunlin is of special concern because of THSR. According to a national poll on December 25, 2006, 49.6% of those who participated in the poll indicated that the government should provide information about the subsidence problem in Yunlin, which is the major outcome of this study. According to our results, currently subsidence in Yunlin has not created excessive angular deflections and reductions of column loading capacity along the THSR rail, but will pose a serious threat if the subsidence is not mitigated. Continual monitoring of subsidences in Yunlin will provide vital data for the safety of THSR.

5 Conclusions

In this article we used leveling, GPS and monitoring wells to collect data to determine subsidence along a section of THSR where subsidence poses a significant threat to its

safety. By dedicated data processing procedures, the subsidence measured from leveling and GPS are consistent to within 1 cm. The subsidence from Stations 210 to 240K is bowl shaped and can be classified into minor, major and moderate subsidence. The sediment compaction measurements at three monitoring wells indicate that the subsidence is attributed largely to compaction occurring at depths from 50 to 300 m, with the major compaction occurring in the depth interval 220–300 m. The major compaction is caused by withdrawal of ground water.

This study shows that geodetic sensors such as leveling and GPS are complementary to the geotechnical sensors deployed in monitoring wells in the determination of subsidence. A geodetic sensor, which is able to measure subsidence as the integrated subsurface compaction (from land surface to the depth of the monitoring well), can be deployed over a large area and the associated data collection is relatively simple and economic. A monitoring well, which is costly, can be deployed at a few selected locations to measure compaction at different depths, which then can be used to explain the mechanisms of subsidence.

Large angular deflections (nearly 1/1,000) have been measured at some THSR columns, but do not exceed the specified upper bound for safety. Also, current subsidence will not reduce the loading capacity of any THSR column in the studied area. Over the past 10 years, the average subsidence rate in Yunlin is 10 cm/year (Figs. 2 and 3). It is shown (Sect. 3.2) that rainfall or perhaps managed artificial recharge of ground water can immediately reduce subsidences. In order to ensure a safe THSR operation, it is advised that (1) subsidence monitoring should be continued to supply vital data for determining the safety of THSR structures, and (2) withdrawal of ground water in Yunlin and other potentially subsidence-prone areas along THSR must be reduced or completely stopped.

Acknowledgment This study is supported by National Science Council (project number: 95-2221-E-009-353), and Water Resource Agency, Department of Economics, Taiwan.

References

Abidin ZH, Djaja R, Darmawan D, Hadi S, Akbar A, Rajiyowiryono H, Sudibyo Y, Meilan I, Kasuma MA, Kahar J, Subarya C (2001) Land subsidence of Jakarta (Indonesia) and its geodetic monitoring system. Nat Hazards 23:365–387

Beutler G, Brockmann E, Dach T, Fridez P, Gurtner W, Hugentobler U, Johnson J, Mervart L, Rothacher M, Schaer S, Springer T, Weber R (2001) Bernese GPS software version 4.2. Astronomical Institute, University of Bern, Bern, 515 pp

Caspary WF (1987) Concepts of network and deformation analysis. Monograph 11, School of Surveying, University of New South Wales, Kensington, NSW, Australia, 183 pp

Dodson AH, Shardlow PJ, Hubbard LCM, Elgered G, Jarlemark POJ (1996) Wet tropospheric effects on precise relative GPS height determination. J Geodesy 70:188–202

Hwang C, Hsiao YS (2003) Orthometric corrections from leveling, gravity, density and elevation data: a case study in Taiwan. J Geodesy 77:279–291

Koch KR (1987) Parameter estimation and hypothesis testing in linear models. Springer, Berlin, 378 pp

Laier JE, Brenner WH (1984) Instrumentation performance in soft clay soils (a case history). In: Yong RN, Townsend FC (eds) Sedimentation consolidation models—prediction and validation. American Society of Civil Engineers, Reston, VA, pp 426–445

Leick A (2004) GPS satellite surveying, 3rd edn. Wiley, New Jersey, 435 pp

Lin ML, Chan JB (1997) A model analysis of ground subsidence of the Taisei-Mailiao area. In: Proceedings of the 7th conference on current research in geotechnical engineering in Taiwan, pp 891–898 (in Chinese)

Liu CS, Hung WC (2006) Taiwan land subsidence monitoring and surveying analysis. Report of Industrial Technology Research Institute (ITRI), Hsinchu (in Chinese)

Liu CH, Pan YW, Liao JJ, Hung WC (2004) Estimating coefficients of volume compressibility from compaction of strata and piezometric changes in a multiaquifer system in west Taiwan. Eng Geol 75:33–47

Motagh M, Djamour Y, Walter TR, Wetzel HU, Zschau J, Arabi S (2007) Land subsidence in Mashhad Valley, northeast Iran: results from InSAR, leveling and GPS. Geophys J Int 168:518–526

Teatini P, Tosi L, Strozzi T, Carbognin L, Wegmuller U, Rizzetto F (2005) Mapping regional land displacements in the Venice coastland by an integrated monitoring system. Remote Sens Environ 98: 403–413

Terzaghi K, Peck RB, Mesri G (1996) Soil mechanics in engineering practice, 3rd edn. Wiley-Interscience, New York, 592 pp

Wolf PR, Ghilani C (2005) Elementary surveying, an introduction to geomatics, 11th edn. Prentice Hall, 944 pp

Zilkoski DB, D'Onofrio JD, Frakes SJ (1997) Guidelines for establishing GPS-derived ellipsoid heights (Standards: 2 cm and 5 cm) version 4.3, NOAA technical memorandum NOS NGS-58, Silver Spring, MD. http://www.ngs.noaa.gov/PUBS_LIB/NGS-58.html